Size-Selective and Epitaxial Electrochemical/Chemical Synthesis of Sulfur-Passivated Cadmium Sulfide Nanocrystals on Graphite

S. Gorer,† J. A. Ganske, J. C. Hemminger, and R. M. Penner*

Contribution from the Institute for Surface and Interface Science and Department of Chemistry, University of California, Irvine, Irvine, California 92679-2025

Received May 14, 1998

Abstract: Cadmium metal nanocrystallites (NCs), prepared on graphite surfaces by electrochemical deposition, are employed as precursors to synthesize core−shell nanoparticles consisting of a crystalline cadmium sulfide (CdS) core and a sulfur or polysulfide shell. Core−shell NCs having a large CdS core (radii R_{CdS} > 40 Å) were prepared by exposing electrodeposited cadmium particles (R_{Cd} > 25 Å) to H_2S at 300 °C, whereas nanoparticles having a smaller CdS core (down to 17 Å) were obtained from cadmium precursor particles via a $Cd(OH)_2$ intermediate. For both large-core and small-core CdS nanoparticles, the addition of the sulfur capping layer (ranging in thickness from 5 to 30 Å) occurred during exposure to H_2S at 300 °C. Transmission electron microscopy (TEM) and selected area electron diffraction (SAED) data show that the synthesis of CdS NCs proceeded on a particle-by-particle basis such that the particle size and monodispersity of the CdS core were directly related to those of the cadmium metal precursor particles electrodeposited in the first step of the synthesis. The CdS cores of these particles were found by electron diffraction to be epitaxially aligned with the hexagonal periodicity of the graphite surface and oriented with the *c*-axis of the wurtzite unit cell perpendicular to the surface. The low-temperature photoluminescence (PL) spectra for CdS nanocrystals without the sulfur capping layer were dominated by broad trap state emission peaks. In contrast, the PL spectra for sulfur-passivated CdS NCs were characterized by a prominent exciton emission band and much weaker trap state emission peaks. As the radius of the CdS core was reduced from 50 to 17 Å, the energy of the exciton emission peak shifted from the macroscopic value of 2.56 to 3.1 eV in excellent agreement with the predictions of the Coulomb-corrected, effective mass model.

Introduction

To incorporate semiconductor quantum dots (QDs) into devices such as detectors,[1,2] light-emitting diodes,[1] electroluminescent devices,[3,4] and lasers,[5,6] an electrical contact to the quantum dots is required. This requirement can be met by synthesizing QDs on conductive semiconductor surfaces using either molecular beam epitaxy (MBE) or chemical vapor deposition (CVD). Either MBE or CVD can be employed, for example, to produce epitaxial, defect-free,[7−11] and size monodisperse InAs[9−11] or Ge[12,13] islands on GaAs or silicon surfaces, respectively. The disadvantage of these gas-phase synthetic methods is that the size of the QDs which are synthesized is decided by the lattice mismatch which exists between the deposited material and the single-crystal surface. For this reason, it has not been possible to create size monodisperse islands over a *range* of island sizes for a particular deposited material−substrate system.

Despite this limitation, less progress has been reported in the development of *liquid-phase* synthetic methods for epitaxially depositing semiconductor nanoparticles on conductive surfaces. Stickney and co-workers[14−18] have shown that certain II−VI materials may be built up in an atomic layer by layer fashion in electrolyte solutions by electrochemical deposition. This experiment (electrochemical atomic layer epitaxy, ECALE) is the liquid-phase analogue of MBE in that the electrochemical growth of each atomic layer is self-limiting. ECALE is an excellent method for preparing quantum well structures; however, it has so far not been possible to prepare islands (i.e., QDs) using this approach. Hodes, Rubinstein, and co-workers[19−24] have shown that quantum-confined CdSe islands can be

* Corresponding author. E-mail: rmpenner@uci.edu.
† Present address: Symyx Technology, Santa Clara, CA 95051. E-mail: sgorer@symyx.com.

(1) Greenham, N. C.; Peng, X. G.; Alivisatos, A. P. *Phys. Rev. B* **1996**, *54*, 17628.
(2) Erley, G.; Gorer, S.; Penner, R. M. *Appl. Phys. Lett.* **1998**.
(3) Colvin, V. L.; Schlamp, M. C.; Alivisatos, A. P. *Nature* **1994**, *370*, 354−357.
(4) Dabbousi, B. O.; Bawendi, M. G.; Onitsuka, O.; Rubner, M. F. *Appl. Phys. Lett.* **1995**, *66*, 1316.
(5) Shoji, H.; Makai, K.; Ohtsuka, N.; Sugawara, M.; Uchida, T.; Ischikawa, H. *IEEE Photon. Technol. Lett.* **1995**, *7*, 1385.
(6) Kirstaedter, N.; Ledentsov, N. N.; Grundmann, M.; Bimberg, D.; Ustimov, V. M.; Ruvimov, S. S.; Maximov, P. S. *Electron Lett.* **1994**, *30*, 1416.
(7) Fitzgerald, E. A.; Watson, G. P.; Proano, R. E.; Ast, D. G.; Kirchner, P. D.; Pettit, G. D.; Woodall, J. M. *J. Appl. Phys.* **1989**, *65*, 2220.
(8) Fitzgerald, E. A.; Kirchner, P. D.; Proano, R.; Pettit, G. D.; Woodall, J. M.; Ast, D. G. *Appl. Phys. Lett.* **1988**, *52*, 1496.
(9) Guha, S.; Madhukar, A.; Raykumar, K. C. *Appl. Phys. Lett.* **1990**, *57*, 2110.
(10) Leonard, D.; Kristnamurthy, M.; Reaves, C. M.; Den-Baars, S. P.; Petroff, P. M. *Appl. Phys. Lett.* **1993**, *63*, 3203.
(11) Leonard, D.; Pond, K.; Petroff, P. M. *Phys. Rev. B* **1994**, *50*, 11687.
(12) Eaglesham, D. J.; Cerullo, M. *Phys. Rev. Lett.* **1990**, *64*, 1943.
(13) Mo, Y.-W.; Savage, D. E.; Swartzentruber, B. S.; Lagally, M. G. *Phys. Rev. Lett.* **1990**, *65*, 1020.
(14) Suggs, D. W.; Villegas, I.; Gregory, B. W.; Stickney, J. L. *J. Vac. Sci. Technol., A* **1992**, *10*, 886.
(15) Suggs, D. W.; Stickney, J. L. *Surf. Sci.* **1993**, *290*, 362.
(16) Suggs, D. W.; Stickney, J. L. *Surf. Sci.* **1993**, *290*, 375.
(17) Lister, T. E.; Colletti, L. P.; Stickney, J. L. *Isr. J. Chem.* **1997**, *37*, 287.
(18) Lister, T. E.; Stickney, J. L. *Appl. Surf. Sci.* **1996**, *107*, 153.

S0002-7863(98)01676-X CCC: $15.00
Published on Web 08/28/1998

Scheme 1

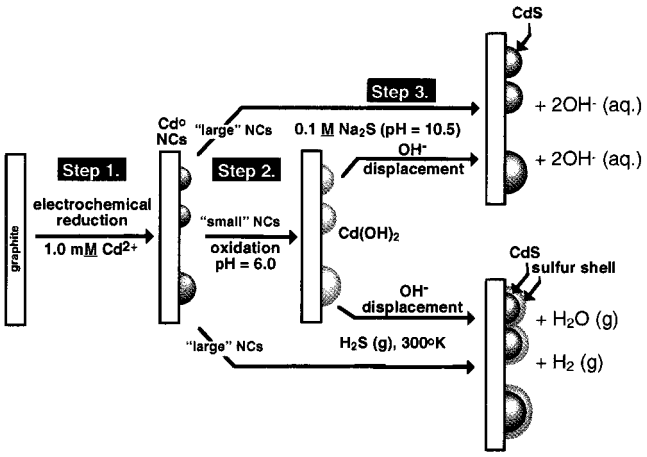

epitaxially electrodeposited onto Au(111) surfaces, that the size of the resulting islands is determined by the interfacial strain energy, and that the lattice constant of the deposited material can be employed to adjust the island size (e.g., using alloys of the type $CdSe_xTe_{1-x}$). Recently,[25] we have described a hybrid electrochemical/chemical (E/C) method for synthesizing CuI nanocrystals on graphite surfaces.[25] The three-step E/C method involves the electrochemical growth of metal nanocrystals (e.g., Cu), the oxidation of these to yield a metal oxide or hydroxide (e.g., Cu_2O), and the displacement of the OH^- or O_2^- with an anion to yield wurtzite-phase CuI nanocrystallites (NCs) (Scheme 1).[25] These CuI nanocrystals were epitaxially aligned with the graphite surface, strongly luminescent at the band edge at room temperature, and narrowly dispersed in size. A key point is that good size monodispersity can be achieved over a range of particle diameters using the E/C approach because the diameter of CuI nanocrystals is determined by the diameter of Cu° precursor nanoparticles, and these electrochemically deposited metal precursor particles possess a narrow size distribution.

Here an E/C procedure for synthesizing core−shell nanostructures consisting of a wurtzite-phase CdS core and a sulfur or polysulfide shell (henceforth, CdS/S) is described. These "core−shell" NCs are deposited with epitaxial registry of the CdS core on the hexagonal graphite surface, and the radius of this CdS core can be adjusted from 17 to 50 Å again using the Cd deposition duration. The synthesis procedure involves three steps: (1) the electrodeposition of cadmium nanoparticles on the graphite surface, (2) the electrochemical oxidation of these nanocrystals, and (3) the conversion of the oxidized intermediate to CdS using gaseous H_2S at 300 °C. A key point is that once the displacement reaction in step 3 is complete, H_2S then decomposes preferentially on the CdS nanocrystals to form a passivating sulfur cap (having a thickness of up to 30 Å) which scavenges the dangling bonds at the surface of the CdS. Previously, several groups have reported methods for preparing *suspensions* of core−shell nanoparticles (including CdS/Cd-$(OH)_2$,[26] CdS/PbS,[27,28] CdSe/ZnS,[29,30] CdSe/CdS,[31] Si/SiO_2,[32−34] CdSe/ZnSe,[35−38] and CdS/HgS/CdS[39−42]), and the layered architecture has been credited with improving both the luminescence properties and the environmental stability of these particles. We report here that the epitaxial sulfur-capped CdS nanocrystals (henceforth, CdS/S) prepared by the E/C method exhibit nearly pure exciton emission spectra whereas uncapped CdS nanocrystals[43] exhibit photoluminescence spectra in which trap state emission predominates.

Experimental Methods

A. Cadmium Sulfide Nanocrystallite Synthesis. The following procedure was employed for the synthesis of CdS/S core−shell NCs: (1) Cd^0 NCs which were narrowly dispersed in size were electrochemically deposited from an aqueous 1.0 mM CdF_2, 0.1 M NaF (pH ∼ 6.2) plating solution onto a freshly cleaved graphite basal plane surface, (2) Cd^0 NCs spontaneously oxidized in the plating solution at open circuit (large Cd^0 NCs having radii greater than 30 Å were incompletely oxidized *vide infra*, and (3) the graphite surface was removed from the electrochemical cell, rinsed with nanopure water, and transferred to a quartz tube furnace in which it was heated in flowing H_2S at 300 °C and atmospheric pressure for 10 min. As described in detail below, this procedure yielded CdS/S core−shell NCs having a wurtzite core 17−50 Å in radius and a sulfur shell up to 30 Å in thickness. As in the case of CuI, the size and monodispersity of the CdS core of these CdS/S NCs were determined by the corresponding properties of the $Cd(OH)_2$ (or Cd^0) NCs which were deposited in step 1.

Further details regarding the pulsed, overpotential deposition (pulsed OPD) of Cd^0 (step 1) are as follows: A platinum wire counter electrode and mercurous sulfate (MSE) reference electrodes were employed, a deposition overpotential of −350 mV (vs the reversible Nernst potential for 1.0 mM Cd^{2+}/Cd^0) was used, and current transients for the deposition of cadmium metal were corrected for background nonfaradaic current.

B. X-ray Photoelectron Spectroscopy. X-ray photoelectron spectroscopy (XPS) was carried out using an ESCALAB MKII

(19) Golan, Y.; Alperson, B.; Hutchison, J. L.; Hodes, G.; Rubinstein, I. *Adv. Mater.* **1997**, *9*, 236 ff.
(20) Golan, Y.; Margulis, L.; Rubinstein, I.; Hodes, G. *Langmuir* **1992**, *8*, 749−752.
(21) Golan, Y.; Margulis, L.; Hodes, G.; Rubinstein, I.; Hutchison, J. L. *Surf. Sci.* **1994**, *311*, L633−L640.
(22) Golan, Y.; Hutchison, J. L.; Rubinstein, I.; Hodes, G. *Adv. Mater.* **1996**, *8*, 631.
(23) Golan, Y.; Hodes, G.; Rubinstein, I. *J. Phys. Chem.* **1996**, *100*, 2220−2228.
(24) Golan, Y.; Terovanesyan, E.; Manassen, Y.; Margulis, L.; Hodes, G.; Rubinstein, I.; Bithell, E. G.; Hutchison, J. L. *Surf. Sci.* **1996**, *350*, 277−284.
(25) Hsiao, G. S.; Anderson, M. G.; Gorer, S.; Harris, D.; Penner, R. M. *J. Am. Chem. Soc.* **1997**, *119*, 1439−1448.
(26) Spanhel, L.; Hasse, M.; Weller, H.; Henglein, A. *J. Am. Chem. Soc.* **1987**, *109*, 5649.
(27) Zhou, H. S.; Sasahara, H.; Honma, I.; Komiyama, H.; Haus, J. W. *Chem. Mater.* **1994**, *6*, 1534−1541.
(28) Zhou, H. S.; Honma, I.; Komiyama, H.; Haus, J. W. *J. Phys. Chem.* **1993**, *97*, 895−901.
(29) Kortan, A. R.; Hull, R.; Opila, R. L.; Bawendi, M. G.; Steigerwald, M. L.; Carroll, P. J.; Brus, L. E. *J. Am. Chem. Soc.* **1990**, *112*, 1327−1332.
(30) Hines, M. A.; Guyot-Sionnest, P. *J. Phys. Chem.* **1996**, *100*, 468.
(31) Peng, X. G.; Schlamp, M. C.; Kadavanich, A. V.; Alivisatos, A. P. *J. Am. Chem. Soc.* **1997**, *119*, 7019.
(32) Schuppler, S.; Friedman, S. L.; Marcus, M. A.; Adler, D. L.; Xie, Y. H.; Ross, F. M.; Harris, T. D.; Brown, W. L.; Chabal, Y. J.; Brus, L. E.; Citrin, P. H. *Phys. Rev. Lett.* **1994**, *72*, 2648.
(33) Schuppler, S.; Friedman, S. L.; Marcus, M. A.; Adler, D. L.; Xie, Y. H.; Ross, F. M.; Chabal, Y. J.; Harris, T. D.; Brus, L. E.; Brown, W. L.; Chaban, E. E.; Szajowski, P. F.; Christman, S. B.; Citrin, P. H. *Phys. Rev. B* **1995**, *52*, 4910.
(34) Wilson, W. L.; Szajowski, P. F.; Brus, L. E. *Science* **1993**, *262*, 1242−1244.
(35) Hoener, C. E.; Allan, K. A.; Bard, A. J.; Campion, A.; Fox, M. A.; Mallouk, T. E.; Webber, S. E.; White, J. M. *J. Phys. Chem.* **1992**, *96*, 3812.
(36) Danek, M.; Jensen, K. F.; Murray, C. B.; Bawendi, M. G. *J. Cryst. Growth* **1994**, *145*, 714−720.
(37) Danek, M.; Jensen, K. F.; Murray, C. B.; Bawendi, M. G. *Appl. Phys. Lett.* **1994**, *65*, 2795−2797.
(38) Danek, M.; Jensen, K. F.; Murray, C. B.; Bawendi, M. G. *Chem. Mater.* **1996**, *8*, 173−180.
(39) Eychmuller, A.; Hasselbarth, A.; Weller, H. *J. Lumin.* **1992**, *53*, 113−115.
(40) Eychmuller, A.; Mews, A.; Weller, H. *Chem. Phys. Lett.* **1993**, *208*, 59−62.
(41) Mews, A.; Eychmuller, A.; Giersig, M.; Schooss, D.; Weller, H. *J. Phys. Chem.* **1994**, *98*, 934−941.
(42) Mews, A.; Kadavanich, A. V.; Banin, U.; Alivisatos, A. P. *Phys. Rev. B* **1996**, *53*, 13242−13245.
(43) Anderson, M. A.; Gorer, S.; Penner, R. M. *J. Phys. Chem. B* **1997**, *101*, 5895−5899.

photoelectron spectrometer (VG Scientific). The ESCALAB MKII is a multitechnique surface analysis instrument based on an ultrahigh vacuum (UHV) system consisting of three separately pumped, interconnected chambers (sample preparation, fast sample entry, and spectroscopy). The fast entry chamber allowed rapid sample transfer from air to UHV pressures (base pressures during XPS analysis were in the low-to-middle 10^{-10} Torr range). The XPS experiments were performed in the spectroscopy chamber using a standard Mg anode X-ray source (and the Mg Kα photoline at 1253.6 eV) and a 150 mm hemispherical electron energy analyzer. The spectra presented here were carried out using an analyzer pass energy of 20 eV. Under these conditions the spectrometer energy resolution was ~0.8 eV. Samples were prepared by supporting the graphite surface, upon which the Cd NCs were prepared, onto a copper sample holder using conductive colloidal silver paste (Ted Pella, Inc.).

C. Transmission Electron Microscopy and Selected Area Electron Diffraction. Transmission electron microscopy (TEM) and selected area electron diffraction (SAED) data were acquired on CdS/S NCs on the graphite basal plane surface on which they were deposited. A proven method for accomplishing this analysis[25,44−46] is by preparing a working electrode consisting of thin (100−400 Å) graphite flakes (~0.5 mm^2) supported on carbon-coated gold TEM grids (Ted Pella, Inc.). The electrochemical deposition of cadmium was then performed on this electrode using the procedure described above. TEM data were obtained on a Philips EM-200 microscope using an accelerating voltage of 200 keV. Diffraction patterns were obtained at a camera length of 1000 mm using a selected area aperture having a diameter of 10 μm. Following the deposition of cadmium NCs and the open circuit oxidation of these particles in the plating solution, graphite surfaces were removed from the electrochemical cell, rinsed with nanopure water, and transported in air to the TEM for analysis.

D. Fluorescence Microprobe Measurements. Luminescence spectra were acquired using 140 mW continuous wave excitation from an argon ion laser at 351 nm. Power densities of ~200 W cm^{-2} at the sample were typical. Laser light with p-polarization was incident on the sample at Brewster's angle (~60°) from the surface normal. Emission was collected at normal incidence through a 20× Zeiss EpiPlan microscope objective, na = 0.45. The light was then coupled with an f4 lens into an imaging spectrograph (Chromex 250IS, equipped with 1200 and 300 groves mm^{-1} holographic gratings, both 500 nm blaze) which dispersed the light onto a liquid nitrogen-cooled CCD (Princeton Instruments Model LN/1024EUV) having 1024 × 256 pixels. Signals from the 256 pixels arrayed perpendicular to the long axis of the CCD were binned, producing a linear detector with 1024 channels. The pixel-wise resolution of this detector was 0.6 and 2.3 meV using the 1200 and 300 groves mm^{-1} gratings, respectively. The sample was contained in a cryostat cooled with a closed cycle helium refrigerator which permitted control of the sample temperature from ambient temperature down to 20 K. Collection times varied between 0.05 and 30 s.

Results and Discussion

A. E/C Synthesis of CdS/S Core/Shell−NCs. The E/C synthesis of CdS nanocrystals begins with the electrodeposition of cadmium NCs on the graphite surface. Cadmium electrodeposition was carried out by applying a potential step to a graphite electrode immersed in aqueous 1.0 mM CdF_2, 0.1 M NaF (pH ~6.2). As in previous work involving silver,[47,48] copper,[25] and platinum,[44] the amplitude of this step was adjusted to yield a large deposition overpotential, $\eta = E_{dep} - E^{o'}_{Cd/Cd^{2+}}$, of −300 mV. A typical 100 ms current−time transient acquired during the deposition of cadmium using this procedure is shown in Figure 1A. Following the application of a plating pulse, the current decayed monotonically and, for times longer than 10 ms, in direct proportion to $t^{-1/2}$ (see the inset). This response is expected for a reaction occurring at the diffusion-controlled rate on a planar electrode surface.[49] The diffusion coefficient for Cd^{2+} calculated from the slope of the straight line indicated in the I vs $t^{-1/2}$ plot of Figure 1A is 2.4 × 10^{-6} cm^2 s^{-1}. At times shorter than 10 ms, the inset shows that the measured deposition current is lower than that predicted for diffusion-controlled deposition. This lower initial rate is a manifestation of slow Cd^{2+} reduction kinetics,[49] and it is not observed for the deposition of other metals (e.g., platinum[44]) having more facile interfacial electron-transfer kinetics. In previous work involving the deposition of silver[47] and platinum[44] nanoparticles on graphite, it was shown that the mechanism of deposition involved instantaneous nucleation (on the 5 ms time scale) and the subsequent growth of these nuclei at diffusion control on the graphite surface.[44,47] This deposition mechanism leads to

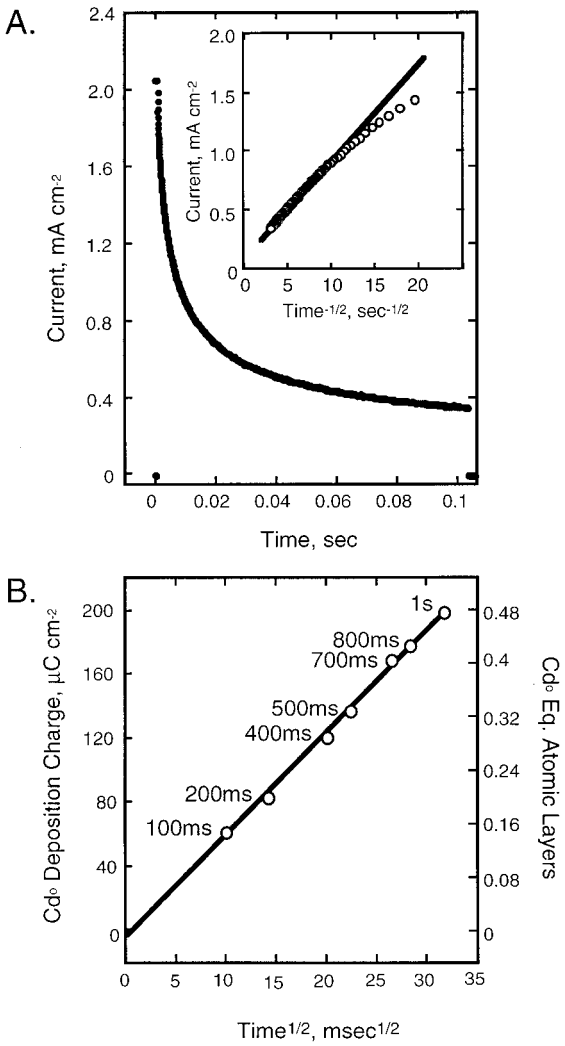

Figure 1. (A) Current vs time for the potentiostatic deposition of cadmium nanocrystals from 1.0 mM CdF_2, 0.1 M NaF (pH ~6.2) onto highly oriented pyrolytic graphite. The potential was stepped to −490 mV vs NHE in this case. Inset: Current versus $(time)^{-1/2}$ for the same data. (B) Quantity of deposited cadmium metal (as coulombs, and as cadmium monolayers) versus $(time)^{1/2}$.

(44) Zoval, J. V.; Lee, J.; Gorer, S.; Penner, R. M. *J. Phys. Chem.* **1998**, *102*, 1166.
(45) Nyffenegger, R. M.; Craft, B.; Shaaban, M.; Gorer, S.; Penner, R. M. *Chem. Mater.*, in press.
(46) Gorer, S.; Hsiao, G. S.; Anderson, M. G.; Stiger, R. M.; Lee, J.; Penner, R. M. *Electrochim. Acta*, in press.
(47) Zoval, J. V.; Stiger, R. M.; Biernacki, P. R.; Penner, R. M. *J. Phys. Chem.* **1996**, *100*, 837−844.
(48) Zoval, J. V.; Biernacki, P. R.; Penner, R. M. *Anal. Chem.* **1996**, *68*, 1585−1592.
(49) Bard, A. J.; Faulkner, L. R. *Electrochemical Methods: Fundementals and Applications*; John Wiley & Sons: New York, 1980.

metal nanoparticles which are narrowly dispersed in size, and—in conjunction with the fact that individual cadmium nanoparticles are converted into CdS nanoparticles—it accounts for the size monodispersity of the CdS nanocrystals which are obtained using this E/C method.

Because cadmium electrodeposition occurs at the diffusion-controlled rate, the quantity of electrodeposited cadmium (measured coulometrically) should be directly proportional to the square root of the plating duration.[49] This is shown to be true in Figure 1B in which the total cadmium deposition charge is plotted against (deposition time)$^{1/2}$ for seven experiments. Because the areal density of particles (i.e., the number of particles per unit area) is not affected by the plating time, this parameter provides a means for controlling the diameter of cadmium nanoparticles, and the diameter of the CdS nanocrystals which are derived from these precursors (as shown below in Figure 5).

B. Transmission Electron Microscopy/Selected Area Electron Diffraction. The E/C synthesis of CdS nanocrystals was carried out on electron transparent graphite flakes in order to monitor the composition of intermediate and product nanoparticles using transmission electron microscopy and selected area electron diffraction. Incipient CdS nanocrystals were investigated at two junctures during their synthesis: first, following the deposition of cadmium nanoparticles and the exposure of these nanoparticles to the plating solution at open circuit, and second, following the exposure of these nanoparticles (which are either Cd^0 or $Cd(OH)_2$) to H_2S at 300 °C. The oxide-free cadmium nanoparticles which are directly produced by electrochemical plating in step 1 could not be probed by TEM and SAED because the surfaces of these nanoparticles quickly (in less than 5 s) and spontaneously oxidized in the plating solution at open circuit to form $Cd(OH)_2$ (vide infra).

The TEM image of Figure 2A shows a 1000 Å × 1000 Å area at the edge of an electron transparent graphite flake. Within the confines of the flake, particles with a mean diameter of 18 Å are visible adjacent to these steps as well as in the middle of terraces. These nanoparticles are assigned a composition of $Cd(OH)_2$ on the basis of SAED patterns such as that shown in Figure 2B:[50] Shown here are data which were acquired for a 10 μm diameter region centered at the location shown in Figure 2A and encompassing several thousand nanoparticles similar to those seen there. In addition to a hexagonal array of diffraction spots which derive from the hexagonal periodicity of the graphite flake, two diffuse rings are visible. These are assigned to [100] and [110] diffraction from hexagonal $Cd(OH)_2$ (International Centre for Diffraction Data, ICDD no. 31-0228) with *d* spacings of 3.0264 and 1.7475 Å, respectively, as shown schematically in Figure 2C. Weaker diffraction from [200] (d = 1.5138 Å) of $Cd(OH)_2$ was also discernible in the raw data for this and other SAED patterns for the oxidized cadmium intermediate. Diffraction from [002] was not observed, and the extinction of this diffraction in the data of Figure 4B implies that $Cd(OH)_2$ nanocrystals are oriented with their *c*-axes perpendicular to the plane of the graphite surface.

The SAED pattern of Figure 2B was typical of those obtained for oxidized cadmium nanoparticles smaller than 40 Å in diameter. For nanoparticles larger than 60 Å, a different powder diffraction pattern assignable to FCC cadmium metal (ICDD 05-0674) was obtained as previously described.[43] Thus, for larger cadmium nanoparticles produced in step 1, oxidation to $Cd(OH)_2$ did not proceed to completion under the conditions of our experiment. Oxidized cadmium nanoparticles of intermediate size having a mean diameter in the range from 20 to 60 Å exhibited diffraction assignable to either FCC cadmium or $Cd(OH)_2$.

The diffraction *rings* observed for [100] and [110] result from diffraction from an ensemble of $Cd(OH)_2$ nanocrystals which possess no in-plane orientational preference. The absence of an epitaxial orientation for $Cd(OH)_2$ nanocrystals would seem to be easily explained: The lattice mismatch between the $Cd(OH)_2$ lattice (a = 3.4947 Å) and graphite(0001) ($2d_{[100]}$ = 2 × 2.1386 Å = 4.2772 Å) is 27%. However, the interaction between $Cd(OH)_2$ nanoparticles and the graphite surface involves van der Waals forces, and long-range coincidences between these two lattices might induce an epitaxial alignment even in the absence of a good direct lattice match. Figure 3 shows a calculation of the energy of a rigid, two-layer-thick $Cd(OH)_2$ island (containing 182 atoms) on a rigid HOPG(0001) surface (containing 1882 atoms in two layers) as a function of the azimuthal orientation of the island on the surface.[51] A (0001) structure for the surface of the $Cd(OH)_2$ particle in contact with the graphite surface has been assumed since this is the orientation required by the known *c*-axis orientation of these particles. No significant energetic wells—corresponding to coincidences of the $Cd(OH)_2$ lattice with the graphite surface—are seen in this calculation.

Following TEM imaging and diffraction analysis, this sample was transferred from the TEM to a tube furnace in which it was heated to 300 °C and exposed to flowing H_2S for 10 min. From a thermodynamic standpoint, nanocrystals of either Cd^0 or $Cd(OH)_2$ are likely to be converted to CdS under these reaction conditions. The conversion of the larger, Cd^0 nanoparticles to CdS (via Cd^0 (s) + H_2S (g) H_2 (g) + CdS (s)) is exothermic ($\Delta H_r \approx -34$ kcal mol^{-1}); the reaction of $Cd(OH)_2$ to form CdS (via $Cd(OH)_2$ (s) + H_2S (g) + H_2O (g) + CdS (s)) is slightly exothermic ($\Delta H_r \approx -15$ kcal mol^{-1}) and entropically favorable.

Direct evidence of the conversion from $Cd(OH)_2$ to CdS is available by comparison of the TEM image of Figure 2D with that of Figure 2A, acquired at the same location on the graphite flake. Nanoparticles are again visible, and a careful comparison with Figure 2A shows that the positions of individual nanoparticles are the same in Figure 2D as in Figure 2A to within 5 Å. Distinctive patterns of nanoparticles—marked with the lower case letters u, v, and w—are useful in making this comparison. Evidence that the nanoparticles seen in the TEM image of Figure 2D are CdS is provided by the SAED pattern of Figure 2E in which the diffraction rings seen in Figure 2B were replaced by diffraction spots at *d* spacings of 3.59 and 1.79 Å consistent with [100] and [200] for wurtzite-phase CdS (ICDD no. 41-1049). As was seen for $Cd(OH)_2$, diffraction from [002] (the second most intense in the X-ray powder pattern for CdS) was absent, suggesting the *c*-axes of these nanocrystals were oriented perpendicular to the plane of the graphite surface. However, in contrast to the SAED data for $Cd(OH)_2$, in-plane diffraction from [100] and [200] for CdS yielded *spots*, not rings. These spots are generated when the diffracted electrons from thousands of wurtzite-phase CdS nanocrystals, possessing the same orientation on the graphite surface, interfere constructively. This result is explained by an epitaxial ordering of CdS nanocrystals with the hexagonal periodicity of the graphite surface. A

(50) The very existence of insoluble $Cd(OH)_2$ on this surface is unexpected since the thermodynamic product of oxidation at this pH (~6.0) is Cd^{2+}.

(51) The energy of the island has been calculated as a function of island angle on the surface by applying a generic Lennard-Jones (L-J) 6−12 potential. The resulting energy versus angle data have been normalized by the well depth, ϵ^o, of the L-J potential (350 K).

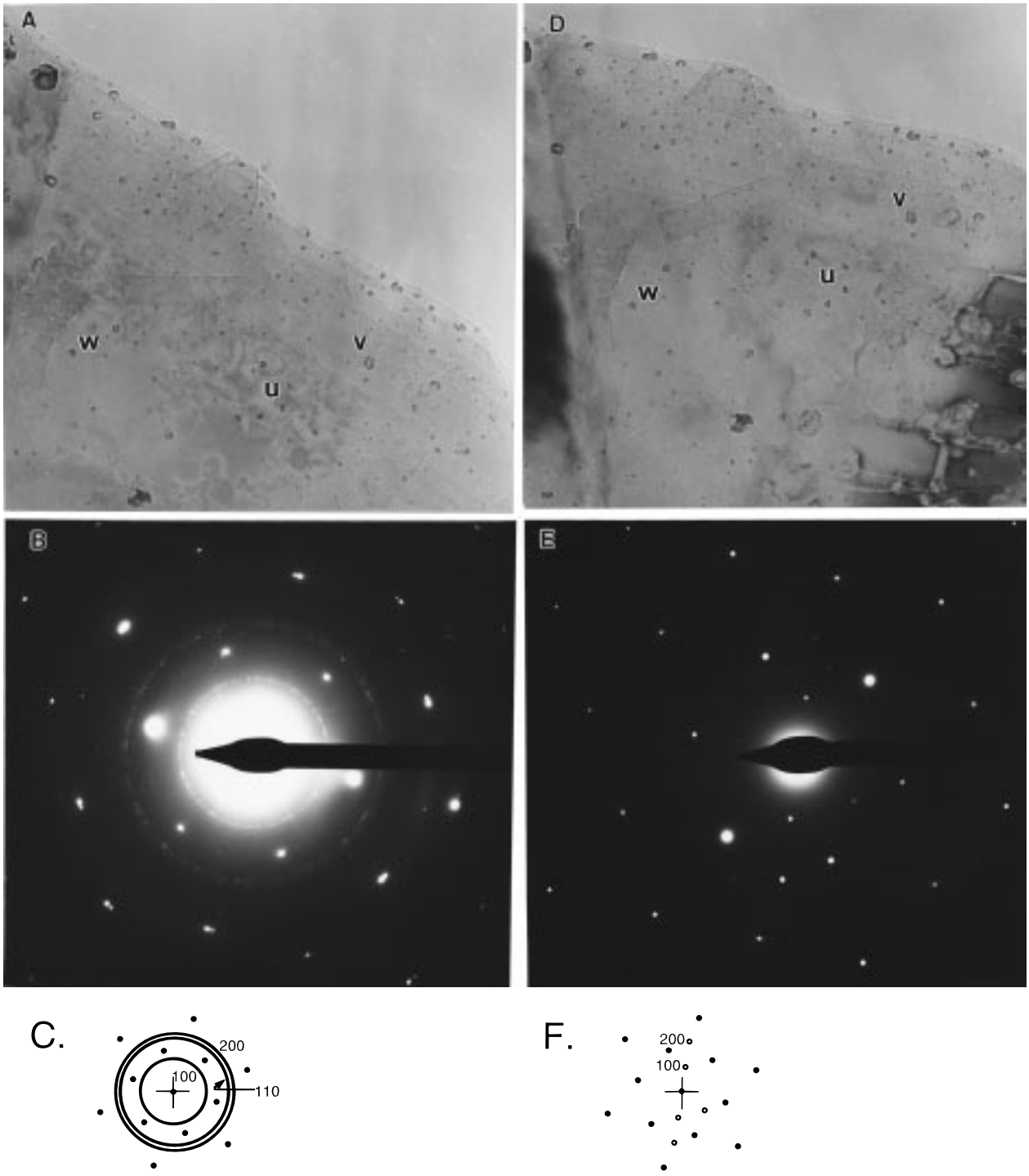

Figure 2. Transmission electron microscope (TEM) images (A, D) and selected area electron diffraction (SAED) data (B, E) for nanocrystals of $Cd(OH)_2$ and CdS. (A) TEM image of a 1000 Å × 1000 Å area near the edge of an electron transparent graphite flake following the deposition of cadmium nanocrystals, and open circuit electrochemical oxidation to form nanocrystals of $Cd(OH)_2$. Lower case letters (e.g., u, v, w) indicate distinctive clusters of nanocrystallites. (B) SAED pattern for a 10 μm diameter region centered at the position on the sample shown in (A). In addition to hexagonal spots derived from the in-plane hexagonal periodicity of the graphite surface, two broken rings of diffracted electrons are also visible which derive from the hexagonal $Cd(OH)_2$ nanocrystals (space group $P\bar{3}m1$ (164)). In fact, a third faint ring of diffracted electron intensity is visible in the raw data just outside of the outermost ring visible in this figure. These diffractions are assigned in (C). (C) Schematic diagram of, and diffraction assignments for, the SAED pattern of (B) from International Centre for Diffraction Data File No. 31-0228. The *d* spacings responsible for each ring are [200] 1.514 Å, [110] 1.748 Å, and [100] 3.026 Å. (D) TEM image of the same 1000 Å × 1000 Å area shown in (A) following the exposure of $Cd(OH)_2$ to H_2S at 300 °C for 20 min. The lowercase letters indicate the same clusters of NCs marked in (A). (E) SAED pattern centered at the position on the sample shown in (D). The diffraction rings seen in (B) have been replaced by spots which are assigned to wurzite-phase CdS (space group $P6_3mc$ (186)). These diffractions are assigned in (F). (F) Schematic diagram of, and diffraction assignments for, the SAED pattern of (E) from International Centre for Diffraction Data File No. 41-1049. The *d* spacings responsible for each ring are [200] 1.793 Å and [100] 3.586 Å.

surprising aspect of this result is that this alignment with the graphite surface occurs following the exposure of $Cd(OH)_2$ nanoparticles, which are clearly *not* epitaxial, to H_2S. In the E/C synthesis of epitaxial CuI nanocrystals reported earlier,[25]

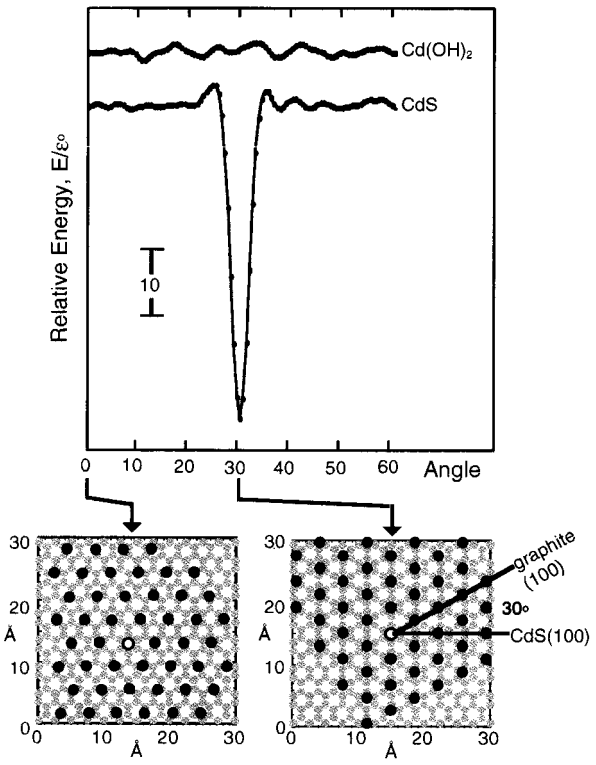

Figure 3. Calculation of the normalized energy, $E/\epsilon°$, of $Cd(OH)_2$ and CdS islands on graphite(0001) where ϵ^o is the well depth of the Lennard-Jones interaction potential with the surface. Each island was approximately 25 Å in diameter and consisted of 126 atoms partitioned into two layers of equal size; the graphite surface consisted of a total of 1882 atoms partitioned between two layers. For both compounds, (0001) faces of the island were assumed to be in contact with the graphite surface in accordance with the SAED data. Shown below left is the starting point for the calculation showing atoms of the topmost carbon monolayer (gray) and atoms of the first CdS monolayer (black atoms). At right is shown the minimum energy position for the CdS island corresponding to a rotation from the initial position of 30°.

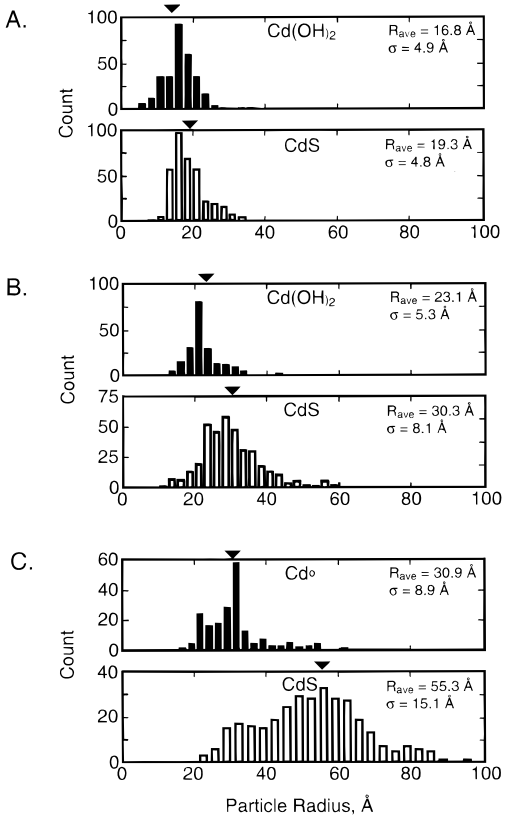

Figure 4. Histograms of particle radii for $Cd(OH)_2$, Cd^0, and CdS nanocrystals constructed from TEM image data. These histograms are organized into three pairs A−C corresponding to three E/C synthesis experiments. For each experiment are shown histograms for both the intermediate (either $Cd(OH)_2$ or Cd^0) and the product CdS derived from that intermediate. The label attached to each histogram reflects the identity of the particles which were analyzed as determined using SAED analysis.

nanocrystals of both the oxidized copper intermediate, Cu_2O, and CuI were epitaxial. The data of Figure 2 show that an epitaxial alignment of the product (CdS) nanocrystals can be obtained from nanocrystals of an oxidized intermediate ($Cd(OH)_2$) which are not epitaxial.

The origin of the epitaxial alignment of CdS nanocrystals on the graphite surface is the small lattice mismatch of 3.2% which exists for cadmium or sulfur atoms in the (0001) plane of CdS ($a = 4.141$ Å) with the hexagonal periodicity of the graphite surface ($2d_{[100]} = 4.2772$ Å). The resulting coincidence between these lattices leads to a pronounced minimum in the energy vs angle plot of Figure 3 at an angle of 30°, and no other significant energetic minima are seen in this plot. SAED patterns identical to that of Figure 2E were obtained following the exposure of large (diameter >80 Å) *cadmium* nanoparticles to H_2S at 300 °C.

Collectively, diffraction and TEM data like those shown in Figure 2 permit four conclusions: (1) Small (diameter <35 Å) cadmium nanoparticles are cleanly oxidized in the cadmium plating solution at open circuit to yield hexagonal $Cd(OH)_2$ nanoparticles. The *c*-axes of these particles are oriented perpendicular to the plane of the graphite surface, but they possess no in-plane alignment. (2) Large (diameter >80 Å) cadmium nanoparticles are incompletely oxidized and SAED patterns are dominated by diffraction from FCC cadmium; these nanoparticles possess no preferred orientation on the graphite surface. (3) Exposure of either of these intermediates to H_2S at 300 °C produces wurtzite-phase CdS nanoparticles which are epitaxially aligned with the hexagonal periodicity of the graphite surface. (4) The conversion from $Cd(OH)_2$ to CdS occurs on a particle-by-particle basis, and this chemical transformation occurs without significant translation of these nanoparticles on the graphite surface.

The transformation from the oxidized cadmium intermediate to CdS was also followed using TEM for nanoparticles of various sizes. Typical histograms of particle diameters are shown in Figure 4, and data for a larger number of experiments are summarized in the plot of mean particle diameter versus cadmium deposition charge shown in Figure 5 (the data points marked A−C correspond to the histograms of Figure 4A−C). Since the molar volumes of CdS and $Cd(OH)_2$ are nearly identical (29.98 vs 30.57 $cm^3\ mol^{-1}$, respectively), the mean particle diameter and the width of the diameter distribution should remain constant during the transformation from $Cd(OH)_2$ to CdS. As shown both in the histogram of Figure 4A and in Figure 5, this expectation is realized for the smallest nanoparticles we have investigated having diameters of ∼34−38 Å. For slightly larger nanoparticles ($\text{diameter}_{Cd(OH)_2}$ >40 Å), however, the measured diameter of CdS nanoparticles was consistently larger by 8−20 Å than the diameter of the $Cd(OH)_2$ "parent" nanoparticles, and an increase in the width of the diameter distribution was also apparent (Figure 4B). These increases in diameter and in polydispersity are observed even though it is clear, on the basis of data such as those shown in

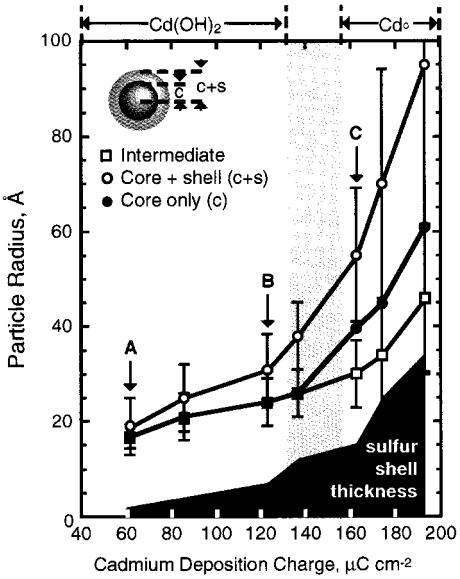

Figure 5. *Experimentally measured* mean radii for oxidized cadmium nanoparticles (□), and for CdS nanocrystals (○). Also shown is the *predicted* radius of CdS nanocrystals calculated from the measured diameter of the oxidized nanoparticles (●). The top of the solid black region is the difference between the experimentally measured CdS radius and the predicted CdS radius. This difference approximates the thickness of a sulfur layer on the surface of the CdS nanocrystal. The samples labeled with upper case A, B, and C correspond to the same samples for which histograms are shown in Figure 4. The labels shown at the top of this figure (either $Cd(OH)_2$ or Cd^0) indicate the identity of the intermediate particles which were analyzed as determined using SAED analysis.

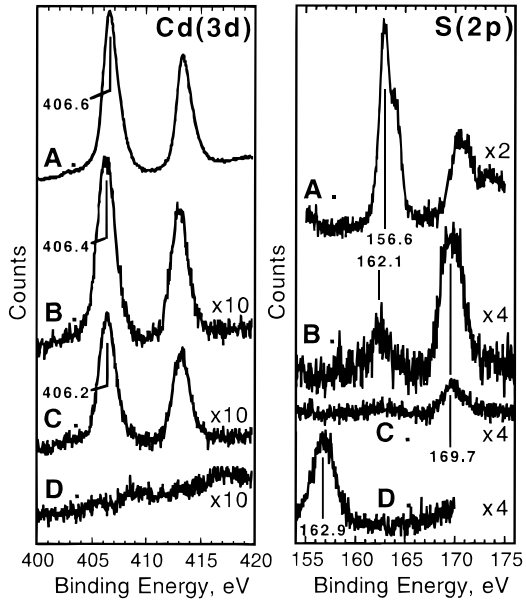

Figure 6. XPS spectra showing Cd(3d) and S(2p) regions for four samples: (A) CdS(0001) single-crystal surface following etching in dilute HCl to remove the sulfur surface layer. (B) Cd^0 nanocrystals following deposition and open circuit oxidation. (C) CdS nanocrystals prepared by conversion of Cd^0 nanoparticles to CdS in aqueous 0.10 M Na_2S, at pH 10 for several minutes. (D) CdS nanocrystals prepared by conversion of Cd^0 nanoparticles to CdS in flowing H_2S at 300 °C for 20 min. These spectra are corrected for the relative sensitivities of cadmium vs sulfur. The mean radius for samples of nanoparticles (B, C, and D) was in the range from 30 to 40 Å.

Figure 2, that this displacement reaction is occurring on a particle-by-particle basis. As indicated above, the largest intermediates we have examined—with diameters larger than 80 Å—exhibited SAED patterns for FCC cadmium metal. If these particles are assumed to be pure cadmium metal (i.e., without a $Cd(OH)_2$ shell), then a 32% increase in the particle diameter is expected upon conversion to CdS on the basis of the larger molar volume of CdS relative to Cd^0 (29.98 vs 13.01 $cm^3\ mol^{-1}$, respectively). The expected diameter of CdS nanoparticles based on the diameter of the oxidized cadmium precursor particles (Figure 5, open squares) is plotted as the filled circles in Figure 5. The diameter of the CdS nanoparticles *actually measured* from TEM images (Figure 5, open circles) is larger by 30−70 Å than these predictions, and again, a larger than expected increase in the width of the distribution is seen (see, for example, Figure 4C). In other words, a larger than expected increase in the particle diameter, and the particle polydispersity, was seen for all but the smallest $Cd(OH)_2$ nanoparticles upon conversion to CdS. These increases are well outside our error bars for measuring these two parameters from the TEM data.

On the basis of the X-ray photoelectron spectroscopic data for $Cd(OH)_2$ and CdS nanoparticles discussed below, the "anomalous" particle size increase seen during conversion to CdS is caused by the growth of a sulfur shell on the surface of CdS nanocrystals. This sulfur shell is not detected in SAED measurements, indicating that it is amorphous. The approximate thickness of this sulfur shell, plotted at the bottom of Figure 5, is equal to the "excess" radius of the particle—where the excess radius is the difference between the mean particle radius following exposure to H_2S and the expected CdS core diameter which was calculated using the mean radius of the Cd^0 or $Cd(OH)_2$ intermediate and the molar volumes of Cd^0, $Cd(OH)_2$, and CdS. This comparison reveals that the sulfur capping layer is thin (<10 Å) for small CdS nanocrystals (CdS core diameter <45 Å) but up to 30 Å in thickness for the largest CdS nanocrystals having core diameters of more than 100 Å. It is not yet clear why—for identical exposures to H_2S—a thicker sulfur layer deposits on large nanocrystals. In section D below, we show that this capping layer has a pronounced effect on the photoluminescence characteristics of the CdS nanocrystals.

C. X-ray Photoelectron Spectroscopy (XPS). The surface chemical composition of incipient CdS nanoparticles can be monitored for the oxidized cadmium intermediate, following the conversion of these intermediate particles to CdS using XPS because these nanoparticles are in intimate contact with the conductive graphite surface. However, because just 2% of the graphite surface is covered by nanoparticles in a typical E/C synthesis, it was necessary to confine XPS studies to large particles (e.g., core diameter ≥40 Å for CdS/S) in order to obtain an acceptable signal-to-noise ratio. Attention is focused on the Cd(3d) and S(2p) regions of these spectra in Figure 6.

As already discussed, CdS nanoparticles can be obtained in two different ways from nanoparticles of an oxidized cadmium intermediate: Liquid-phase conversion in aqueous ~0.2 M Na_2S (pH ~ 10),[43] and gas-phase conversion in flowing H_2S at 300 °C (this work). Both "types" of CdS have been investigated by XPS in this study as well as nanoparticles of the oxidized cadmium intermediate. Finally, the cadmium-terminated (0001) surface of a large CdS single crystal, prepared by etching in 5% HCl for 15 s, was examined. In the Cd(3d) region, appreciable cadmium signals are seen both for nanoparticles of the oxidized cadmium intermediate and for nanocrystals of the liquid-phase-converted CdS. Relative to the $Cd(3d_{5/2})$ binding energy of the CdS(0001) surface, these peaks are shifted to lower binding energy by 0.2 and 0.4 eV, respectively, qualitatively as seen previously.[52] No cadmium XPS signal was seen,

however, for gas-phase-converted samples (Figure 6D) despite the fact that such samples reproducibly yielded clean, single-crystal diffraction patterns for CdS.

In the S(2p) region, the binding energy of the $2p_{3/2}$ peak in the spectrum of the single-crystal CdS surface was 162.9 eV, and this is consistent with previous work.[52,53] Integration of Cd($3d_{5/2}$) and S(2p) peaks yields an approximate Cd:S stoichiometry of 1.6:1—qualitatively as expected for the (0001) surface following removal of sulfur by an HCl etch. A higher binding energy sulfur peak, assigned to sulfate, was observed for all samples in the range from 169 to 170 eV. This was traced to glassware contamination by sulfate caused by a H_2SO_4 cleaning bath. A sulfide peak was not observed for nanoparticles of the oxidized cadmium intermediate, but a peak at ~162 eV was seen for CdS nanocrystals prepared by liquid-phase conversion. Again, this binding energy is close to that seen for S(2p) for CdS nanocrystals in previous work.[53] The surface of liquid-phase-synthesized CdS nanocrystals was cadmium rich with a Cd:S ratio of 2.5−3.0.

CdS nanocrystals prepared by displacement in H_2S exhibited a very low binding energy peak at 156.6 eV which is 4 eV below the chemical shift range for sulfur in any of its oxidation states. This peak is attributed either to sulfur (i.e., oligomeric sulfur) or to polysulfide (polymeric sulfur), and it is proposed that the low binding energy is caused by negative charging of these presumably electrically insulating, sulfur-capped nanoparticles. The formation of this sulfur cap requires the decomposition of H_2S at 300 °C according to the reaction $H_2S(g) \rightleftharpoons H_2(g) + S(s)$. This reaction is nearly thermoneutral ($\Delta H_r = 7.1$ kcal mol^{-1}),[54] so in the absence of a significant partial pressure of H_2 it is readily conceivable that this decomposition occurs spontaneously. Especially in light of this fact, it is important to note that the deposition of sulfur onto these surfaces during the gas-phase displacement reaction occurs *selectively* on the CdS nanocrystals: No sulfur was detectable by XPS following the exposure of clean graphite surfaces to H_2S under the conditions of the displacement reaction.

The attenuation length for 0.8 keV electrons in sulfur is 15−20 Å.[55] Thus, the fact that no cadmium is detected by XPS suggests that CdS nanocrystals prepared by exposure to H_2S are covered with a layer of sulfur which is more than ~30 Å thick. The sample probed in Figure 6C was prepared using, on the basis of the data of Figure 6, sulfur shell thicknesses in the 25−45 Å range.

D. Photoluminence Characterization. Low-temperature (20 K) photoluminence (PL) spectra were acquired for graphite-supported CdS nanocrystals using a fluorescence microprobe which enabled the acquisition of spectra from small regions of the graphite surface. In this study, 200 μm diameter regions of the surface encompassing hundreds of thousands of CdS nanocrystals were probed; CdS nanocrystals were excited using 3.53 eV light (351 nm).

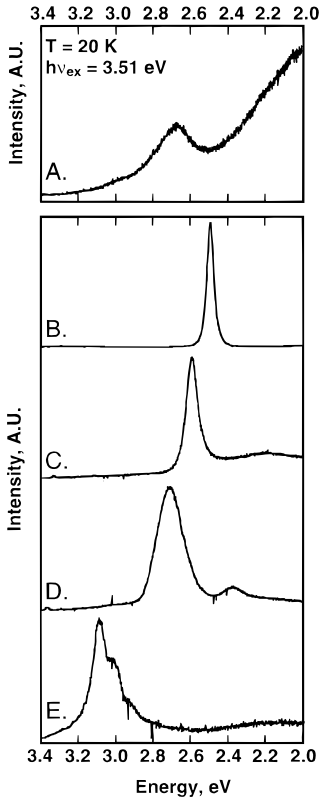

Figure 7. Photoluminescence (PL) spectra for CdS nanoparticles prepared using the E/C method (A, C−E), and for a CdS single crystal (B). All spectra were obtained at 20 K with 3.53 eV (351 nm) excitation. Excitation power densities were near 200 W cm^{-2}; peak PL intensities were normalized. (A) CdS nanocrystals (radius ~40 Å) prepared by conversion of Cd^0 nanoparticles to CdS in aqueous 0.10 M Na_2S, at pH 10 for several minutes. (B) CdS(0001) single-crystal surface following etching in dilute HCl to remove the sulfur surface layer. (C, D) CdS nanocrystals prepared by E/C synthesis with conversion to CdS in flowing H_2S at 300 °C for 20 min. The mean and standard deviations for the CdS core radii of these nanocrystals (inferred from TEM analysis; see Figure 5) were as follows: (C) 40.Å ± 9 Å, (D) 24 Å ± 5.0 Å, and (E) 17 Å ± 2.5 Å.

A PL spectrum for E/C synthesized CdS nanocrystals (diameter ~80 Å) prepared by immersing $Cd(OH)_2$ nanoparticles into aqueous 0.1 M Na_2S, pH 10.5, is shown in Figure 7A. This procedure yields CdS nanocrystals which are epitaxially aligned with the graphite surface,[43] but it is apparent from Figure 1A that PL spectra from these liquid-phase-converted particles are dominated by emission from trap states. For CdS nanocrystals synthesized in aqueous solutions, these trap states have most often been attributed to surface stoichiometric excesses of Cd^{2+} (or, equivalently, S^{2-} vacancies).[56−58] As already noted above, XPS spectra for these liquid-phase-converted CdS nanocrystals show an excess of Cd^{2+} relative to S^{2-}.

(52) Niles, D. W.; Herdt, G.; Al-Jassim, M. *J. Appl. Phys.* **1997**, *81*, 1978.

(53) Colvin, V. L.; Goldstein, A. N.; Alivisatos, A. P. *J. Am. Chem. Soc.* **1992**, *114*, 5221−5230.

(54) Chase, M. *JANAF Thermodynamic Tables*, 2nd. ed.; NIST: Washington, DC, 1985; Vol. 3.

(55) The inelastic mean free path (IMFP) for photoelectrons in sulfur can be calculated using an empirical equation (TPP-2) developed by Powell and co-workers (Powell, C. J. *Surf. Sci.* **1994**, *299/300*, 34.). TPP-2, which can be parametrized for the physical and electronic properties of sulfur and the photoelectron energy (~0.8 keV, in this case), yields an IMFP value of 20 Å. The attenuation length, AL, for photoelectrons will be somewhat shorter than this, in the range from 15 to 20 Å. Using these values, and the XPS spectrum of liquid-phase-synthesized CdS nanocrystals (Figure 4C) as a basis for comparison, the signal-to-noise ratio for the Cd$3d_{5/2}$ peak of gas-phase-converted CdS nanocrystals, S/N_{gas}, can be estimated using $S/N_{gas} = S/N_{liquid}e^{-x/AL}$. If AL = 20 Å, x (the sulfur layer thickness) = 30 Å, and $S/N_{liquid} \approx 10$, then a value for S/N_{gas} of 2.2 is obtained. For AL = 15 Å, S/N_{gas} drops to 1.4. Cadmium XPS signals of this magnitude would be difficult to detect on the undulating baseline seen in the cadmium XPS spectrum of Figure 4D.

(56) Chestnoy, N.; Harris, T. D.; Hull, R.; Brus, L. E. *J. Phys. Chem.* **1986**, *90*, 3393.

(57) Dannhauser, T.; O′Neil, M.; Johansson, K.; Whitten, D.; McLendon, G. *J. Phys. Chem.* **1986**, *90*, 6074.

(58) Johansson, K.; Cowdery, R.; O'Neil, M.; Rehm, J.; McLendon, G.; Marchetti, A.; Whitten, D. G. *Isr. J. Chem.* **1993**, *33*, 67.

PL spectra for CdS nanocrystals prepared by gas-phase displacement of OH^- (as water) from $Cd(OH)_2$ using H_2S are shown in Figure 7C−E. In contrast to CdS prepared by liquid-phase displacement, the PL spectra for these nanocrystals are dominated by relatively sharp and blue-shifted exciton emission peaks. The reduced intensity of red-shifted trap state emission from these samples is attributed to the reaction of surface Cd^{2+} with S^{2-} produced by the decomposition of H_2S on the surface of CdS nanocrystals. Analogous passivation chemistry has been reported for CdS nanocrystals previously. For example, it has been established that exposure of optically "defective" CdS nanocrystals to alkylamines,[57−59] OH^-,[60] and methyl viologen[61]—all of which react with surface Cd^{2+}—preferentially increase the intensity of exciton emission in the PL spectra of these particles.

The blue shift of the peaks seen in the PL spectra of Figure 7C−E can be compared with theoretical predictions. On the basis of the calculations of Kayanuma[62] and the exciton radius of CdS ($a_B = 29$ Å), CdS nanocrystals with radii smaller than $2a_B$ or 58 Å should conform to the predictions of the strong confinement model:[62,63]

$$\Delta E = \frac{\hbar^2\pi^2}{2R^2}\left[\frac{1}{m_e} + \frac{1}{m_h}\right] - \frac{1.786e^2}{\epsilon R} - 0.248E^*_{Ry} \qquad (1)$$

where ΔE is the blue shift in the exciton peak energy for nanocrystals of radius R, m_e and m_h are the effective masses of electrons and holes, ϵ is the dielectric constant of CdS, and E^*_{Ry} is the effective Rydberg energy of the exciton.[64] The predictions of eq 1, however, must be considered approximate because of the assumptions implicit in the strong confinement model,[62,63] and because bulk materials properties of CdS (i.e., m_e, m_h, and ϵ) are employed in the calculation. In Figure 8, eq 1 is plotted as the solid line and it is apparent that our experimentally measured emission energies fall close to this prediction. Conservatively, this agreement permits the conclusion that neither electrons nor holes are deeply trapped.

In fact, the agreement with the strong confinement model seen here is much better than in several previous studies of the PL from CdS nanocrystals embedded in glass and Nafion matrixes.[65−68] In this earlier work, the disparities with eq 1 were greatest for nanocrystals smaller than 40 Å in radius. Wang and Herron,[68] for example, reported that experimentally measured blue shifts were smaller than predicted by eq 1 by 250 meV for $R = 20$ Å CdS nanocrystals. The key difference compared with this earlier work may be the medium in which the spectroscopy is carried out: In the Wang and Herron study, for example, CdS nanocrystals were synthesized and investigated in the perfluorinated ionomer Nafion whereas our spectroscopic measurements are carried out in high vacuum (for the smallest CdS nanocrystals investigated here, the thickness of the sulfur shell is insignificant). Qualitatively, penetration of the electron wave function into the medium surrounding the nanocrystal will be greater for a condensed phase such as Nafion, leading to a weakening of the quantum size effect. This "incomplete confinement" of the electron is not factored into the simple strong confinement model represented by eq 1, but in the specific case of CdS nanocrystals in silica glasses, Kayanuma et al.[69] have shown quantitatively that incomplete confinement

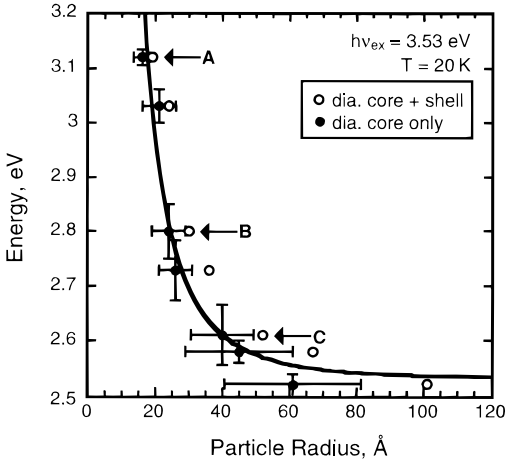

Figure 8. Energy of maximum PL emission versus core radius (●) for CdS nanocrystals following conversion in flowing H_2S at 300 °C for 20 min. Also shown is the total particle radius including sulfur shell (○). Samples labeled A, B, and C correspond to the spectra shown in Figure 7C−E. The solid line shows the band gap energy of CdS as a function of nanocrystal radius calculated using the strong confinement model with no adjustable parameters.

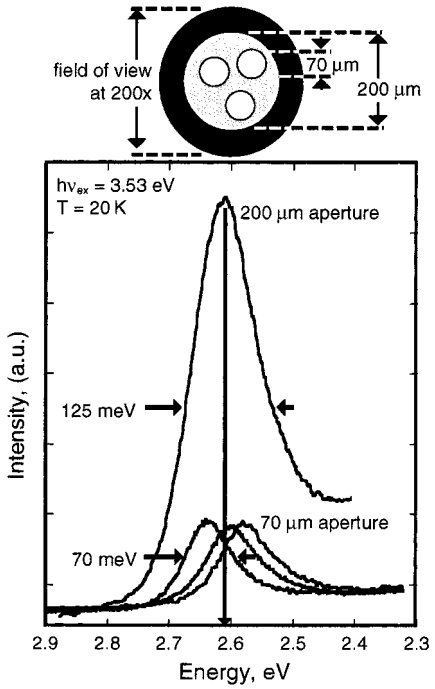

Figure 9. PL spectra for CdS nanocrystals having a mean radius of ~40 Å. These spectra were acquired either from a 200 μm diameter region of the sample surface or from 70 μm diameter regions within the larger 200 μm diameter region as indicated schematically at the top. In general, a narrowing of the exciton emission peak and a shift in its energy are both observed relative to the exciton emission peak in the PL spectrum for the larger region.

(59) Spanhel, L.; Arpac, E.; Schmidt, H. *J. Non-Cryst. Solids* **1992**, *147*, 657−662.
(60) Henglein, A. *Chem. Rev.* **1989**, *89*, 1861.
(61) Ramsden, J. J.; Grätzel, M. *J. Chem. Soc., Faraday Trans.* **1984**, *80*, 919.
(62) Kayanuma, Y. *Phys. Rev. B* **1988**, *38*, 9797.
(63) Brus, L. E. *J. Chem. Phys.* **1984**, *80*, 4403.
(64) The following materials parameters for CdS were employed for the strong confinement calculation: $\epsilon = 5.4$, $m_e/m_o = 0.21$, $m_h/m_o = 0.80$, $m_o = 9.11 \times 10^{-31}$ kg, $E_g(20\text{ K}) = 2.56$ eV, $E^*_{Ryd} = 29$ meV. Reference: Sze, S. M. *The Physics of Semiconductor Devices*, 2nd ed.; John Wiley & Sons: New York.
(65) Borrelli, N. F.; Hall, D. W.; Holland, H. J.; Smith, D. W. *J. Appl. Phys.* **1987**, *61*, 5399.
(66) Ekimov, A. I.; Efros, A. F.; Onushchenko, A. A. *Solid State Commun.* **1985**, *56*, 921.
(67) Shinojima, H.; Yumoto, J.; Uesugi, N.; Omi, S.; Asahara, Y. *Appl. Phys. Lett.* **1989**, *55*, 1519.
(68) Wang, Y.; Herron, N. *Phys. Rev. B* **1990**, *42*, 7253−7255.

can account for the disparities with eq 1 which have been observed experimentally.

A final point involves the widths of the PL lines. The narrowest emission lines (see, for example, Figure 7C) exhibit full widths at half-height of ~125 meV. In a recent study of the PL from single CdS nanocrystals, a homogeneous line width of 15 meV at 20 K was reported for comparable power densities (~200 W cm^{-2}).[70] Thus, inhomogeneous broadening derived from the CdS particle size polydispersity is a possible source of the broader lines seen in Figure 7. This hypothesis is supported by the experiment shown in Figure 8 in which three spectra were acquired from circular, 70 μm diameter regions of a sample within the confines of a larger, 200 μm diameter region. Two effects are observed in these three spectra: First, narrower emission lines having widths of ~70 meV are seen in the spectra from the 70 μm diameter regions, and second, the energy of maximum emission shifted both up and down in energy (as compared with the energy for the 200 μm diameter region) as different regions of the surfaces were sampled. Both of these effects are explained if variations in the CdS nanocrystal diameter are present on the 10−50 μm distance scale on the sample surface. We conclude that further improvement in the size monodispersity of E/C-synthesized nanocrystals is possible, and that these improvements are likely to yield narrower emission lines.

Summary

Electrochemically deposited cadmium nanocrystals have been employed as precursors to synthesize CdS/S core−shell nanocrystals. The nanocrystals obtained using this procedure possess the following attributes: (1) Epitaxial alignment of the CdS core with the hexagonal periodicity of the graphite surface, (2) a sulfur capping layer (amorphous by electron diffraction) which ranges in thickness from <10 to 30 Å, (3) photoluminescence spectra which are characterized by strong exciton emission and much weaker trap state emission, (4) good-to-excellent particle size monodispersity, and, (5) a mean CdS core diameter which is adjustable from 17 to 50 Å.

The deposition of the sulfur capping layer occurs selectively, and "automatically", when the final displacement step of the E/C synthesis is performed at elevated temperatures using H_2S gas. For uncapped CdS nanocrystals prepared by E/C in the liquid phase,[43] the XPS data suggest that strong surface state emission is caused by defect states associated with surface cadmium excesses. It is the removal of these cadmium defects during the deposition of the sulfur cap which is likely responsible for the improvements to the PL spectrum which are seen for CdS/S nanocrystals prepared by gas-phase displacement.

Finally, in combination with our previous E/C synthesis of CuI nanocrystals, this demonstration of the E/C synthesis of high-quality CdS nanocrystals suggests that this new approach may provide a versatile and convenient means by which supported nanocrystals can be prepared for a variety of II−VI and I−VII materials.

Acknowledgment. The authors express their appreciation to Dr. Art Moore of Advanced Ceramics for donations of highly oriented pyrolytic graphite. This work was supported by the Office of Naval Research (Grant N00014-93-1-0757). The following additional sources of funds are also gratefully acknowledged: a Welch Scholarship of the International Union for Vacuum Science (S.G.), The NSF Young Investigator's Program (Grant DMR-9257000), and an A.P. Sloan Fellow, an Arnold and Mabel Beckman Young Investigator award, and a Camille Dreyfus Teacher-Scholar award (R.M.P.).

JA981676L

(69) Kayanuma, Y.; Momiji, H. *Phys. Rev. B* **1990**, *41*, 41.

(70) Tittel, J.; Gohde, W.; Koberling, F.; Basche, T.; Kornowski, A.; Weller, H.; Eychmuller, A. *J. Phys. Chem. B* **1997**, *101*, 3013−3016.